



# Light Limitation and Depth-Variable Sedimentation Drives Vertical Reef Compression on Turbid Coral Reefs

Kyle M. Morgan<sup>1\*</sup>, Molly A. Moynihan<sup>1,2</sup>, Nivedita Sanwani<sup>1</sup> and Adam D. Switzer<sup>1,3</sup>

<sup>1</sup> Asian School of the Environment, Nanyang Technological University, Singapore, Singapore, <sup>2</sup> Earth Observatory of Singapore, Interdisciplinary Graduate School, Nanyang Technological University, Singapore, Singapore, <sup>3</sup> Earth Observatory of Singapore, Nanyang Technological University, Singapore, Singapore

## OPEN ACCESS

### Edited by:

Bert W. Hoeksema,  
Naturalis Biodiversity Center,  
Netherlands

### Reviewed by:

Ross Jones,  
Australian Institute of Marine Science  
(AIMS), Australia  
Tom Bridge,  
Museum of Tropical Queensland,  
Australia

### \*Correspondence:

Kyle M. Morgan  
kmorgan@ntu.edu.sg

### Specialty section:

This article was submitted to  
Marine Ecosystem Ecology,  
a section of the journal  
Frontiers in Marine Science

**Received:** 10 June 2020

**Accepted:** 14 October 2020

**Published:** 20 November 2020

### Citation:

Morgan KM, Moynihan MA,  
Sanwani N and Switzer AD (2020)  
Light Limitation and Depth-Variable  
Sedimentation Drives Vertical Reef  
Compression on Turbid Coral Reefs.  
*Front. Mar. Sci.* 7:571256.  
doi: 10.3389/fmars.2020.571256

Turbid coral reefs experience high suspended sediment loads and low-light conditions that vertically compress the maximum depth of reef growth. Although vertical reef compression is hypothesized to further decrease available coral habitat as environmental conditions on reefs change, its causative processes have not been fully quantified. Here, we present a high-resolution time series of environmental parameters known to influence coral depth distribution (light, turbidity, sedimentation, currents) within reef crest (2–3 m) and reef slope (7 m) habitats on two turbid reefs in Singapore. Light levels on reef crests were low [mean daily light integral (DLI):  $13.9 \pm 5.6$  and  $6.4 \pm 3.0$  mol photons  $m^{-2} day^{-1}$  at Kusu and Hantu, respectively], and light differences between reefs were driven by a 2-fold increase in turbidity at Hantu (typically  $10\text{--}50$  mg  $l^{-1}$ ), despite its similar distance offshore. Light attenuation was rapid ( $K_{dPAR}$ :  $0.49\text{--}0.57$   $m^{-1}$ ) resulting in a shallow euphotic depth of  $<11$  m, and daily fluctuations of up to 8 m. Remote sensing indicates a regional west-to-east gradient in light availability and turbidity across southern Singapore attributed to spatial variability in suspended sediment, chlorophyll-*a* and colored dissolved organic matter. Net sediment accumulation rates were  $\sim 5\%$  of gross rates on reefs ( $9.8\text{--}22.9$  mg  $cm^{-2} day^{-1}$ ) due to the resuspension of sediment by tidal currents, which contribute to the ecological stability of reef crest coral communities. Lower current velocities on the reef slope deposit  $\sim 4$  kg  $m^2$  more silt annually, and result in high soft-sediment benthic cover. Our findings confirm that vertical reef compression is driven from the bottom-up, as the photic zone contracts and fine silt accumulates at depth, reducing available habitat for coral growth. Assuming no further declines in water quality, future sea level rise could decrease the depth distribution of these turbid reefs by a further 8–12%. This highlights the vulnerability of deeper coral communities on turbid reefs to the combined effects of both local anthropogenic inputs and climate-related impacts.

**Keywords:** vertical reef compression, light attenuation, turbidity, sedimentation, Anthropocene, Southeast Asia

## INTRODUCTION

Coral reefs in Southeast (SE) Asia have suffered significant ecological declines (Heery et al., 2018). Widespread reductions in coral cover, species diversity, and reef structural complexity from climate-related disturbances (Guest et al., 2012; Perry and Morgan, 2017; Hughes et al., 2018) are compounded by localized threats to coral reefs, including land-derived siltation and nutrient

loading (Kamp-Nielsen et al., 2002; Baum et al., 2015; Duprey et al., 2020). Declining water quality in the region has been attributed to poorly regulated land-use change, rapid human population growth, and the urbanization of coastal watersheds (Kamp-Nielsen et al., 2002; Syvitski et al., 2005). These anthropogenic stressors can significantly elevate background seawater turbidity and sedimentation, creating low-light conditions, and threaten up to 95% of coastal reefs within SE Asia (Burke et al., 2011). Specifically, the deleterious impacts of elevated turbidity and chronic sedimentation on corals include: (1) reduced coral growth and calcification; (2) smothering of benthic communities and recruitment substrates; and (3) excessive particle loading on coral surfaces (Fabricius, 2005; Erftemeijer et al., 2012; Risk, 2014; Jones et al., 2016; Bainbridge et al., 2018). As a result, coral community compositions on human-impacted reefs have shifted to favor slow-growing and stress-tolerant taxa (Cleary et al., 2016), influencing rates of reef calcification and bioconstruction (Perry and Alvarez-Filip, 2018; Januchowski-Hartley et al., 2020). Localized environmental change is therefore a major present and future issue for SE Asian coral reefs, because the region supports high marine biodiversity (Bellwood and Hughes, 2001) and a very populous coastal zone (Hinrichsen, 2016).

Turbid coral reefs are well-adapted to inhabit areas of naturally high turbidity and low light (e.g., Morgan et al., 2016), and exhibit a tolerance and morphological plasticity to fluctuating abiotic conditions, such as sedimentation, eutrophication, temperature, and light (Anthony et al., 2005; Goodkin et al., 2011; Guest et al., 2012; Morgan et al., 2017). These marginal conditions for coral growth may afford turbid reefs a degree of protection from global climate-related disturbance events (e.g., prolonged ocean warming), as the shading effect of the overlying seawater turbidity can reduce the additive stress of solar irradiance on corals (Morgan et al., 2017; Burt et al., 2020). However, turbid coral reefs remain susceptible to increasing localized inputs from human activities (e.g., seafloor dredging) that may push environmental conditions beyond the threshold for coral growth (Erftemeijer et al., 2012; de Soares, 2020). For example, vertical reef compression, defined here as the shrinking of the total depth range over which photosynthetic corals can grow and reef bioconstruction occurs (e.g., Morgan et al., 2016; Heery et al., 2018), restricts reef-building in turbid waters to between 6–12 m (Goodkin et al., 2011; Heery et al., 2018; Chow et al., 2019). The maximum depth limit of coral growth is primarily dependent on the euphotic depth [i.e., the depth where photosynthetic available radiation (PAR) is 1% of its surface value], below which net photosynthesis occurs. Even minor local increases in suspended sediment load (e.g., 1–10 mg l<sup>-1</sup>), which may have limited direct physiological impacts on the corals themselves, can disproportionately influence coral distribution by attenuating more light and further shallowing the photic floor on these already light-limited reefs (Jones et al., 2015; Storlazzi et al., 2015; Morgan et al., 2020). While a conceptual understanding of vertical reef compression currently exists, the physical environments of turbid reef settings are not well quantified, and greater knowledge of the cause-effect pathways that limit the depth range of coral reef development is needed.

In Singapore, an island megacity that has experienced intense urban development over the past 50 years, long-term monitoring of offshore coral reefs shows divergent trajectories in reef communities associated with depth. Shallow reef crest habitats (2–3 m depth) exhibit stable coral cover and diversity over time, whereas, deeper reef slope corals (7 m depth) have seriously declined, and a transition to soft-sediment benthic substrates has occurred (Guest et al., 2016). These temporal trends in vertical reef compression have been attributed to increasing suspended sediment in offshore waters and accompanying reductions in light (e.g., Lai et al., 2015), but rarely have these parameters been examined together. Furthermore, turbidity regimes on reefs are not yet quantified, and little attention has been given to the physical properties of the suspended sediment themselves, despite the insights they may provide. Here, we present a high-resolution time series of the physical environment for reef crest and reef slope habitats on two turbid reefs in Singapore, where a 27-year record of benthic cover is available, to establish the causative processes driving vertical reef compression. Our field measurements provide an assessment of light, turbidity, sedimentation and currents over a 30-day period and are accompanied by regional remote sensing analysis of ocean optical properties to address the following questions: (1) what are the processes limiting the depth distribution of corals on turbid reefs? (2) how do the physical environments differ between reefs in Singapore? and (3) how will turbid reefs respond to future anthropogenic and climate-related stressors? Given that coastal reefs in SE Asia play a key role in maintaining biodiversity, and that anthropogenic activities in the region continue to intensify, it is crucial to understand the factors that influence habitat availability within turbid settings.

## MATERIALS AND METHODS

### Field Setting

This study was conducted on two fringing coral reefs (Pulau Hantu and Kusu Island) located off the southern coast of Singapore, within the Singapore Strait (**Figure 1**). Pulau Hantu (1.226247°N, 103.747049°E) is sheltered by adjacent islands and reefs at the western side of the Southern Islands group in an area of intense industrialization and ship traffic. Kusu Island (1.225354°N, 103.860104°E), on the eastern side of the Southern Islands group, experiences comparatively higher exposure and lower anthropogenic impacts. The reef platforms are relatively comparable in size (16–30 ha), and cross-reef morphology is characterized by a shallow sand flat (~2–3 m depth), an outer reef crest that supports low-profile sediment-tolerant coral taxa and macroalgae (~2–3 m depth), and a steep fore-reef slope where coral cover is low and soft-sediment dominates at depth (Hilton and Ming, 1999; **Supplementary Figure 1**). The depth of the surrounding seafloor in southern Singapore is relatively consistent (10–15 m), with no major onshore-offshore increase in water depth. High-velocity tidal flows occur throughout the wider Singapore Strait (Chen et al., 2005), and suspended particulate matter in the water column drives episodically chronic sedimentation on reefs (Low and Chou, 1994; Browne et al.,

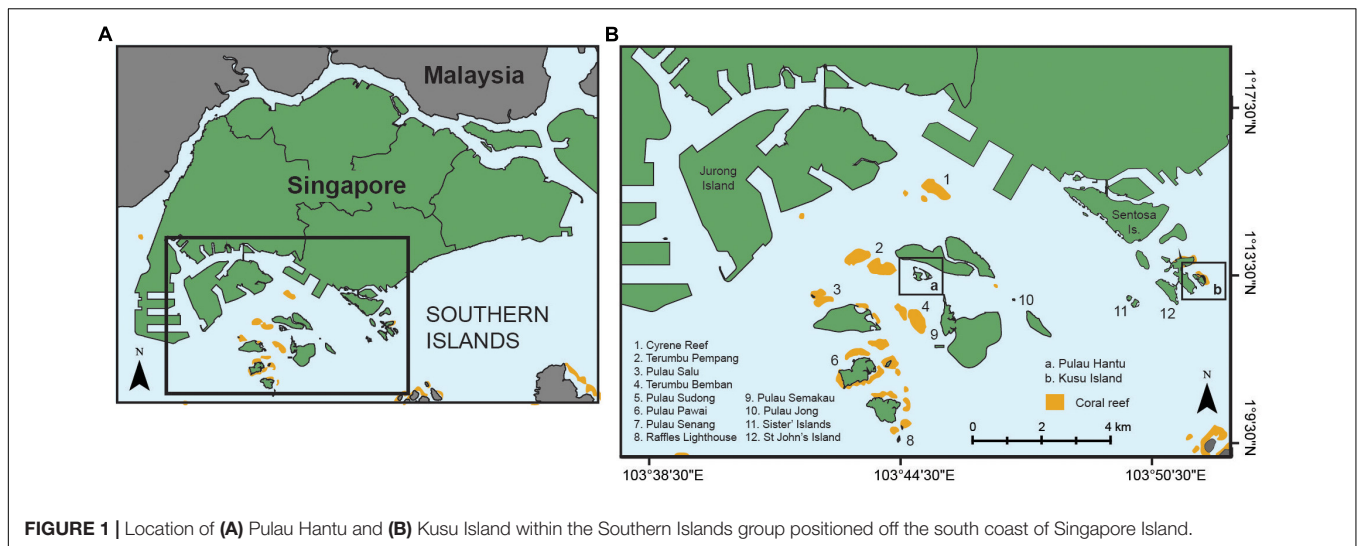


**FIGURE 1** | Location of (A) Pulau Hantu and (B) Kusu Island within the Southern Islands group positioned off the south coast of Singapore Island.

2015). Changes in benthic community structure at Hantu and Kusu reefs over a 27-year time series (see Guest et al., 2016; **Supplementary Figure 2**) suggest that reef crest coral cover at Hantu, following an initial decline in 1997–1998, has remained relatively consistent (24% cover). Coral cover on the reef crest of Kusu demonstrated relatively high cover in 2004–2005 (48% cover). On the reef slope, declines in coral cover to <10% have occurred at both sites alongside a 20% increase in fine sediment cover (Guest et al., 2016).

## Environmental Data Collection

Environmental parameters (light, turbidity, temperature, currents) known to influence coral growth were measured over a 30-day field deployment during the southwest monsoon (August 2018) at Kusu and Hantu reefs. Data was collected using instruments deployed within reef crest (2–3 m depth) and reef slope (7 m depth) habitats comparable to those in long-term benthic monitoring assessments (Guest et al., 2016). Irradiance (PAR) was recorded at each fixed depth every 10 min using pre-calibrated Odyssey<sup>®</sup> submersible light recorders (Shaffer and Beaulieu, 2012). Instantaneous light measurements ( $\mu\text{mol photons m}^{-2} \text{s}^{-1}$ ) were recorded during daylight hours (700–1900 h) and used to calculate a DLI ( $\text{mol photons m}^{-2} \text{day}^{-1}$ ) by summing the 12 h of continuous light at instantaneous levels (per second quantum flux measurements) for every second across the daylight period. For example, instantaneous measurements were multiplied by 600, as there are 600 s in every 10 min sampling period (Jones et al., 2015). Near-bed turbidity (i.e., the degree to which water loses its transparency due to the presence of suspended particulates) was also recorded every 10 min (30 s bursts at 12 Hz) using a horizontal-mounted optical backscatter nephelometer (AQUAlogger<sup>®</sup> 310TY) with in-built pressure sensor deployed 0.3 m from the bed on the reef crest. Values were recorded as Formazin Turbidity Units (FTU) and then converted to suspended sediment concentration (SSC as  $\text{mg l}^{-1}$ ). The conversion factor between FTU and SSC was calculated using the SSC Converter within AQUAtalk software using a linear

relationship ( $R^2 = 0.67$ ) derived from the gravimetric analysis of 26 field water samples filtered through pre-weighed Whatman GF/F filter papers ( $\text{SSC} = \text{FTU} \times 2$ ). Optical sensors (PAR and turbidity) were cleaned weekly during the deployment period to remove biofouling. However, to ensure data quality, only data recorded 3 days after cleaning at Hantu (12 days total) and 4 days after cleaning at Kusu (16 days total) were used for analysis. Reef currents were measured using tilt-current meters (TCM-1: Lowell Instruments) deployed at each site to record current speed ( $\text{cm s}^{-1}$ ), direction (bearing) and water temperature every 10 min (30 s bursts at 4 Hz).

## Time-Series (Running Means Percentile) Analysis

Raw light, turbidity and current time-series data were plotted and all erroneous data values were removed. Mean values for the depth zones across the 30-day period at Kusu and Hantu were calculated and tested for statistical significance using t-tests. However, because environmental conditions on reefs are highly variable, long-term averages may not sufficiently capture short periods of environmental extremes (Jones et al., 2015). To examine the range of likely environmental conditions across the time-scales from hours to weeks, a running means percentile approach was applied to the time-series data to create percentile plots (Jones et al., 2015). We calculated the running means for each environmental parameter over different time periods (30 min, 1 h, 6 h, 12 h, 1–12/16 days, for turbidity and current data; 1–12/16 days for DLI data) and then summarized the results as an average with associated percentile values (100th, 99th, 95th, and 80th for turbidity and current data; 50th, 20th, and 5th for DLI data).

## Reef Sedimentation and Grain Properties

Gross and net sediment accumulation rates were measured within the depth zones at both reefs. To measure gross sediment accumulation (i.e., the downward flux of particles suspended within the water column), three cylindrical tube traps (7 cm

diameter  $\times$  30 cm length) were attached to a stake 0.3 m off the seabed. Net accumulation was measured using SedPods (Field et al., 2013), a flat cylindrical concrete unit (15 cm height  $\times$  15 cm diameter) that replicates a coral/reef surface and allows for resuspension of particles by tidal currents (**Supplementary Figure 1**). Following the 30-day deployment, all traps were capped and retrieved, washed with deionised water to remove salts, dried and weighed to determine sediment mass. Sediment accumulation rates ( $\text{mg cm}^{-2} \text{ day}^{-1}$ ) were calculated by dividing the total amount of dry sediment retained over the deployment period ( $\text{mg day}^{-1}$ ) by the trap surface area ( $\text{cm}^{-2}$ ). To establish physical comparisons between trap material and sediments deposited on corals, sediment was collected directly from the surface of five massive (*Dipsastraea* sp.) and five foliose corals (*Pachyseris* sp.) on the reef slope of Hantu (4–7 m depth) using Pasteur pipettes. Benthic seafloor sediment samples ( $\sim 100$  g) were also collected for comparison at both sites.

The grain size properties of tube trap, SedPod and coral surface sediments ( $< 1$  mm) were measured using laser diffraction analysis (Malvern Mastersizer 3000). Benthic samples, which comprised both fine ( $< 1$  mm) and coarse ( $> 1$  mm) material, were first dry sieved at 0.5 phi intervals, weighed and the proportion of material relative to the total sediment mass was calculated. The separated fine fraction ( $< 63 \mu\text{m}$ ) was analyzed using laser diffraction and the data were combined with the results from sieve analysis to estimate bulk sediment grain statistics using GRADISTAT (Blott and Pye, 2001; Morgan and Kench, 2016). The relative proportions of non-reef derived particles (i.e., clastic), total organic carbon (TOC) and total inorganic carbon (TIC) in the bulk sediment mass were estimated using the loss-on-ignition (LOI) method (Heiri et al., 2001).

## Sediment Deposition and Resuspension Potential

To estimate sediment deposition potential on reefs, the hydrodynamic properties of suspended sediment particles were first established by converting the grain size data to an equivalent settling velocity ( $w_s$ ) using the equations of Gibbs et al. (1971). Sediment deposition potential was then modeled by dividing the average settling velocity of tube trap particles by the current velocities ( $cv$ ) recorded by TCM-1 current meters every 10 min. The percent of time where current velocities fell below the threshold required to keep particles in suspension was then calculated ( $w_s/cv \geq 1.25$ ; Cheng and Chiew, 1999). Resuspension rates were calculated as the difference in sediment accumulation rate ( $\text{mg cm}^{-2} \text{ day}^{-1}$ ) between gross (tube traps) and net sediment accumulation (SedPods). Based on comparisons of the grain size distributions between trap methods deployed at the same location, we estimate the size classes of resuspended sediment by their relative absence on SedPods when compared to tube traps.

## Light Diffuse Attenuation Coefficient ( $K_{dPAR}$ ) and Euphotic Depth ( $Z_d$ )

The diffuse attenuation coefficient of PAR ( $K_{dPAR}$ ) was calculated using daily (at 1200 h) field irradiance data collected from fixed

PAR loggers at reef crest (2–3 m depth) and reef slope sites (7 m depth) (Eq. 1), which were depth-adjusted for daily changes in water level (tidal range: 3.35 m).

$$K_{dPAR}(z) = -\frac{\ln(\text{PAR}(z + dz)) - \ln(\text{PAR}(z))}{dz} \quad (1)$$

The euphotic depth ( $Z_d$ ) is defined as the depth at which 1% of the surface irradiance remains (Saulquin et al., 2013; Macdonald, 2015), and was calculated as in Eq. 2.

$$\text{PAR}(Z) = \text{PAR}(0^-) \times \exp[-K_{dPAR} \times Z] \quad (2)$$

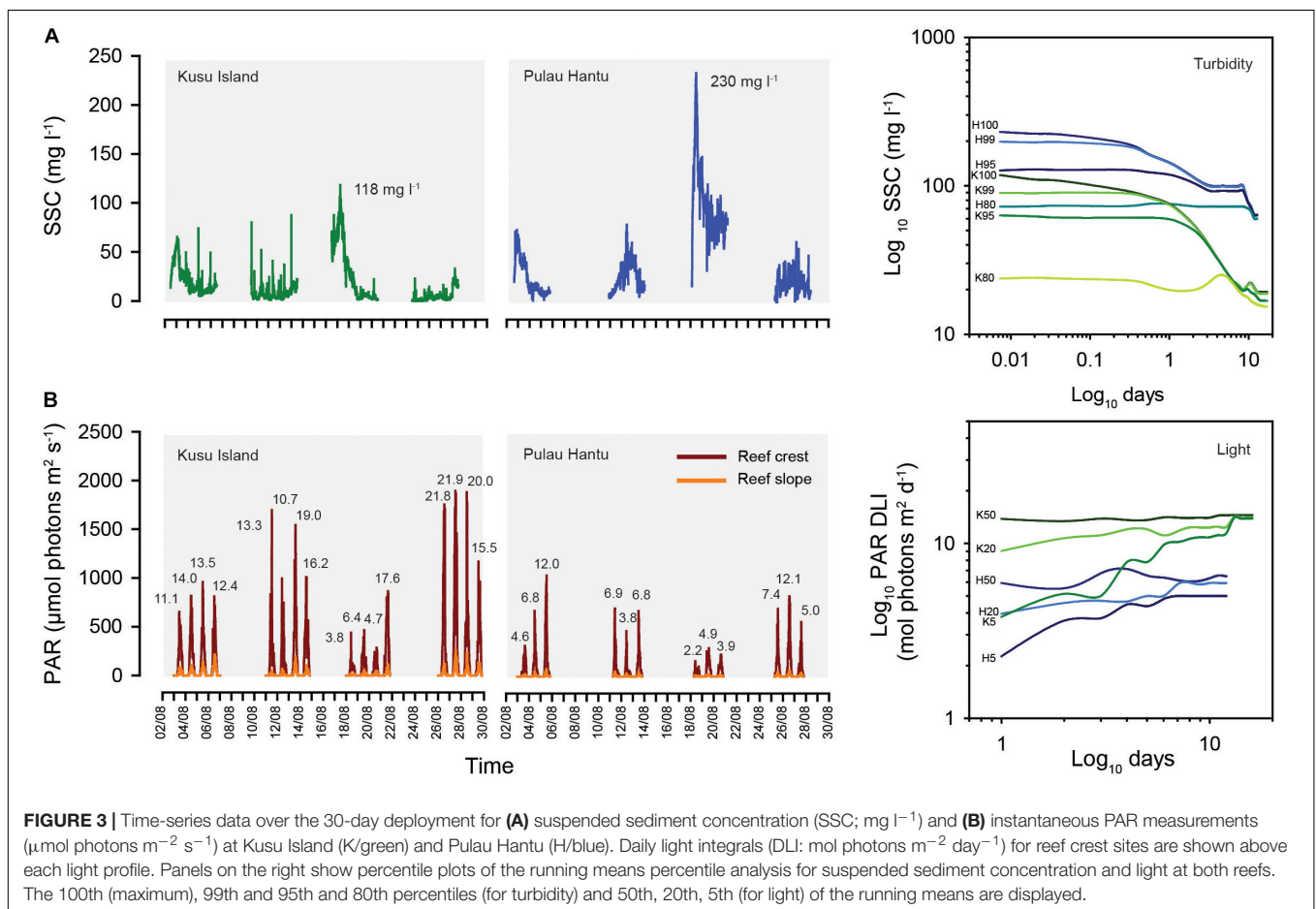
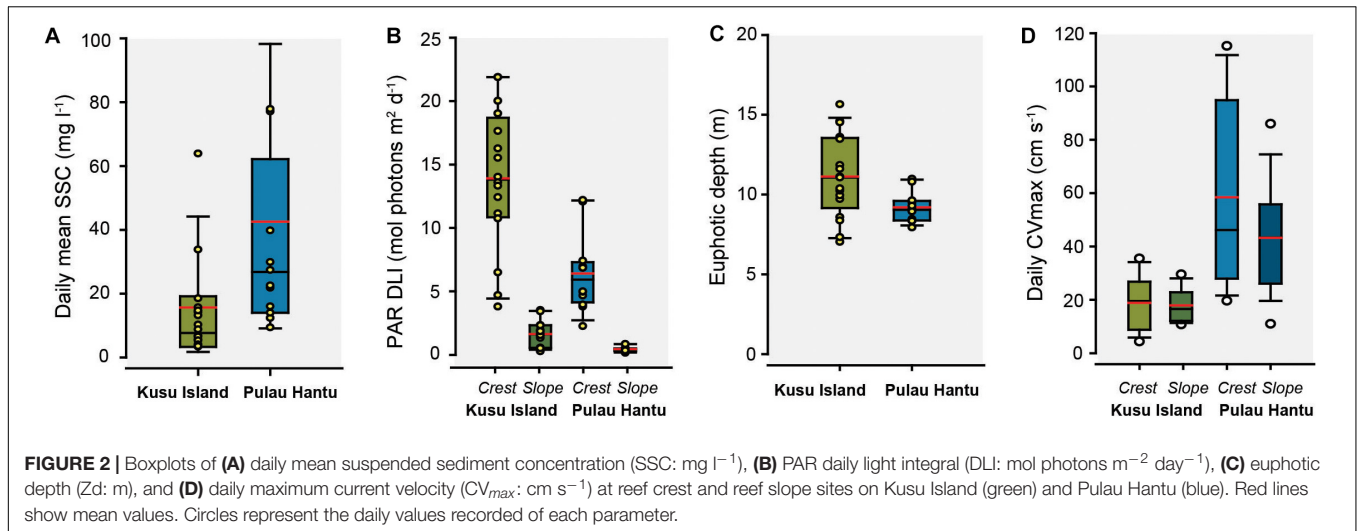
## Remote Sensing Analysis

To examine the spatial distribution of ocean optical properties in southern Singapore, the Level-2 (L2) products of Sentinel-3 Ocean and Land Color Instrument with a 300 m spatial resolution were used. We extracted the following bio-optical constituents from the L2 suite based on the neural network atmospheric correction (Doerffer and Schiller, 2007; Brockmann et al., 2016): (1) algal pigment concentration (chlorophyll-*a* in  $\text{mg m}^{-3}$ ), (2) total suspended matter concentrations (TSM in  $\text{mg l}^{-1}$ ), (3) diffuse attenuation coefficient ( $K_{d490}$  in  $\text{m}^{-1}$ ), (4) water-inherent optical properties of colored dissolved organic matter (CDOM) absorption ( $a_{443}$  at 443 nm in  $\text{m}^{-1}$ ), (5) PAR ( $\mu\text{mol quanta m}^{-2} \text{ s}^{-1}$ ), and (6) euphotic depth (m) derived from  $K_{d490}$ . These parameters were displayed as either actual concentrations of optically active substances, or as their inherent optical properties (IOP). The main neural network derived water-leaving reflectance after atmospheric correction. Subsequently, the IOP module retrieved the absorption and scattering coefficients from the water-leaving reflectance and the concentrations of optically active constituents.

## RESULTS

### Environmental Conditions on Reefs

Temperature was consistent (mean: 29.5°C) between reefs, as well as with depth between habitats ( $p > 0.05$ , *t*-test). Mean turbidity (SSC) across the 30-day deployment period was significantly higher at Hantu ( $42 \pm 40 \text{ mg l}^{-1}$ ) than Kusu ( $16 \pm 19 \text{ mg l}^{-1}$ ) ( $p < 0.05$ , *t*-test), with Hantu experiencing a wider range of turbidity values (Hantu: 0.4–230  $\text{mg l}^{-1}$ ; Kusu: 0.06–118  $\text{mg l}^{-1}$ ) (**Figure 2A**). The time-series data show a substantial peak in SSC (August 17–19) at both sites midway during the study (**Figure 3A**). Running means analysis across multiple time frames (from minutes to weeks) was used to characterize temporal trends across the time-series data. These show that upper percentiles values of SSC (100th, 99th, and 95th) at both sites, which represent periodic pulses in turbidity on reefs, decline with increasing temporal scale (**Figure 3A** and **Supplementary Table 1**). A faster decline in these values was observed at Kusu, indicating lower background SSC once short-term turbidity peaks were smoothed. In comparison, the 80th and 50th (median) percentiles were relatively consistent at both reefs and were substantially lower at Kusu compared to Hantu. Mean turbidity values



derived from running means across the full range of time-scales were 2-fold lower at Kusu ( $11.5\text{--}15.6 \text{ mg l}^{-1}$ ) than at Hantu ( $40\text{--}42.5 \text{ mg l}^{-1}$ ). Collectively, running means percentile analysis shows pronounced separation in turbidity regimes between the reefs.

Both reefs experienced 12 h of daylight (0700–1900 h). The daily maximum irradiance (instantaneous PAR) on the reef crest peaked at approximately solar noon, reaching 1024 and  $2196 \mu\text{mol photons m}^{-2} \text{ s}^{-1}$  at Hantu and Kusu, respectively (Figure 3B). Mean daily maximum irradiance exhibited high

variability across the deployment period, and was significantly higher at Kusu ( $1052 \pm 591 \mu\text{mol photons m}^{-2} \text{ s}^{-1}$ ) than at Hantu ( $542 \pm 265 \mu\text{mol photons m}^{-2} \text{ s}^{-1}$ ) ( $p < 0.05$ ,  $t$ -test). This translated into substantially higher mean DLI values at the reef crest of Kusu ( $13.9 \pm 5.6 \text{ mol photons m}^{-2} \text{ day}^{-1}$ ) compared to Hantu ( $6.4 \pm 3.0 \text{ mol photons m}^{-2} \text{ day}^{-1}$ ) (Figure 2B). Within reefs, both reef slope sites recorded low mean daily maximum instantaneous PAR (Kusu:  $113 \pm 72 \mu\text{mol photons m}^{-2} \text{ s}^{-1}$ ; Hantu:  $37 \pm 18 \mu\text{mol photons m}^{-2} \text{ s}^{-1}$ ) and low mean DLI values (Kusu:  $1.6 \pm 1.0 \mu\text{mol m}^{-2} \text{ s}^{-1}$ ; Hantu:  $0.44 \pm 0.2 \mu\text{mol m}^{-2} \text{ s}^{-1}$ ). Over the deployment period, reef slope sites experienced very low-light conditions ( $\leq 0.8$  DLI) on 5 of the 16 days at Kusu and 11 of the 12 days at Hantu. These values corresponded with periodic increases in SSC ( $> 50 \text{ mg l}^{-1}$ ), which also reduced reef crest DLI values (Figure 3B). Running means analysis (days to weeks) of DLI values show that the 50th percentile (median) is relatively consistent over varying temporal resolutions (Figure 3B and Supplementary Table 2). Whereas the 20th and 5th percentile present an upward trend in agreement with the upper percentile turbidity values at these same sites. There are clear differences in light conditions between reefs, with Kusu characterized by higher light levels and less temporal variability.

Daily  $K_d_{\text{PAR}}$  (taken at 1200 h) shows rapid light attenuation across the deployment period with average  $K_d_{\text{PAR}}$  values ranging between  $0.49 \pm 0.13 \text{ m}^{-1}$  and  $0.57 \pm 0.10 \text{ m}^{-1}$  at Kusu and Hantu, respectively. We also observed daily shifts in the euphotic depth (Figure 4). There were differences in the amount of light attenuation variability between sites, where light penetration on Hantu fluctuated within a substantially narrower envelope than at Kusu. When PAR is reduced to 1% of the surface irradiance ( $Z_d$ ), the euphotic depth ranged between 7.0 and 15.6 m depth (mean:  $11.1 \pm 2.5 \text{ m}$ ) at Kusu, and 7.94 and 10.99 m (mean:  $9.2 \pm 0.9 \text{ m}$ ) at Hantu (Figures 2C, 4).

Maximum daily current velocities (daily  $CV_{\text{max}}$ ) at Hantu were higher than those recorded at Kusu, at both the reef crest and reef slope (Figure 2D). Maximum current conditions have a greater influence on reef sediment dynamics than “normal” (mean) conditions. At Hantu, daily  $CV_{\text{max}}$  on the reef crest reached a peak velocity of  $119 \text{ cm}^{-1} \text{ s}^{-1}$  following low tide, and recorded crest velocities were more variable than those on the reef slope (reef crest:  $17.6$ – $119 \text{ cm}^{-1} \text{ s}^{-1}$ ; reef slope:  $6$ – $91 \text{ cm}^{-1} \text{ s}^{-1}$ ) (Figure 2D). However, averaged daily  $CV_{\text{max}}$  at Hantu were similar between the crest ( $58 \pm 34 \text{ cm}^{-1} \text{ s}^{-1}$ ) and slope ( $43 \pm 20 \text{ cm}^{-1} \text{ s}^{-1}$ ). In comparison, daily  $CV_{\text{max}}$  at Kusu varied over a smaller range (reef crest:  $10$ – $30.5 \text{ cm}^{-1} \text{ s}^{-1}$ ; reef slope:  $3.5$ – $35 \text{ cm}^{-1} \text{ s}^{-1}$ ) and did not align to individual tidal phases, but was higher during periods of increased tidal range (Figure 5A). Averaged daily  $CV_{\text{max}}$  velocities at Kusu were the same between the crest and slope ( $18 \text{ cm}^{-1} \text{ s}^{-1}$ ). Running means percentile analysis (100th, 99th, and 95th) show declines in current velocity with increasing temporal resolution, and higher current velocities at Hantu compared to Kusu (Figure 5 and Supplementary Table 3). Within reefs, upper percentiles exhibited separation in current velocities between depth zones, particularly at Kusu, where velocities were higher at the reef crest than on the reef slope. At Hantu, the separation between

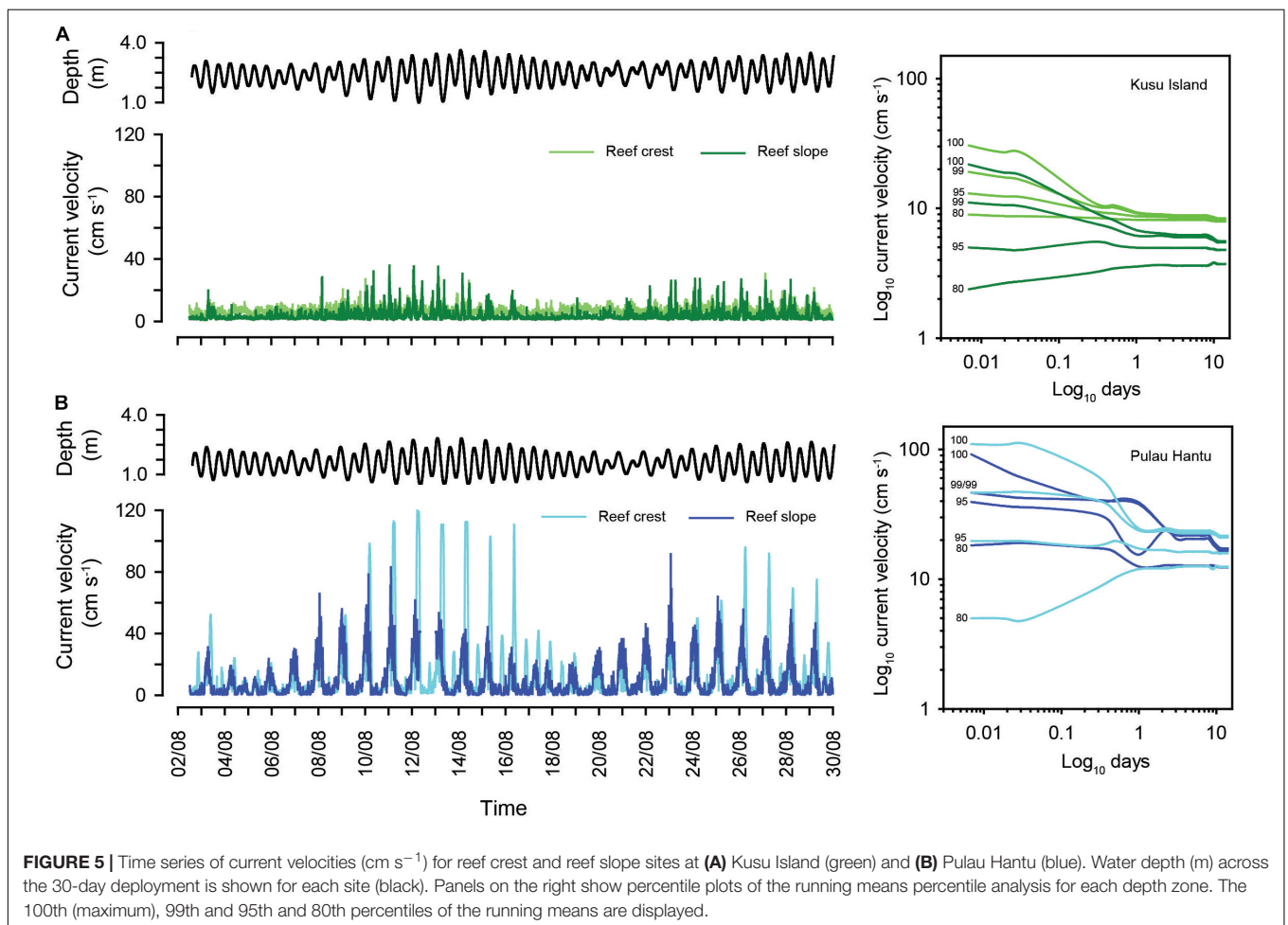
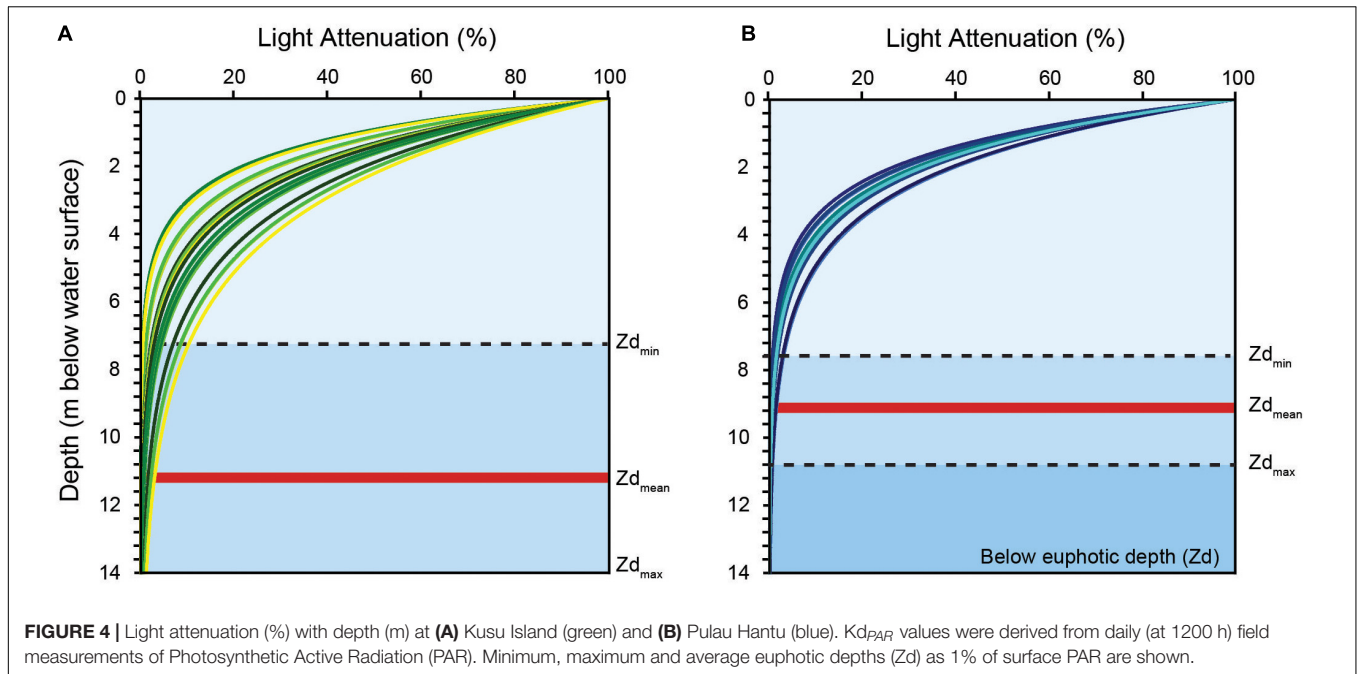
depth zones is not as clear, because although reef crest sites generally experience higher velocities over finer time-scales, they become similar when coarser running average time-scales are applied (Figure 5B).

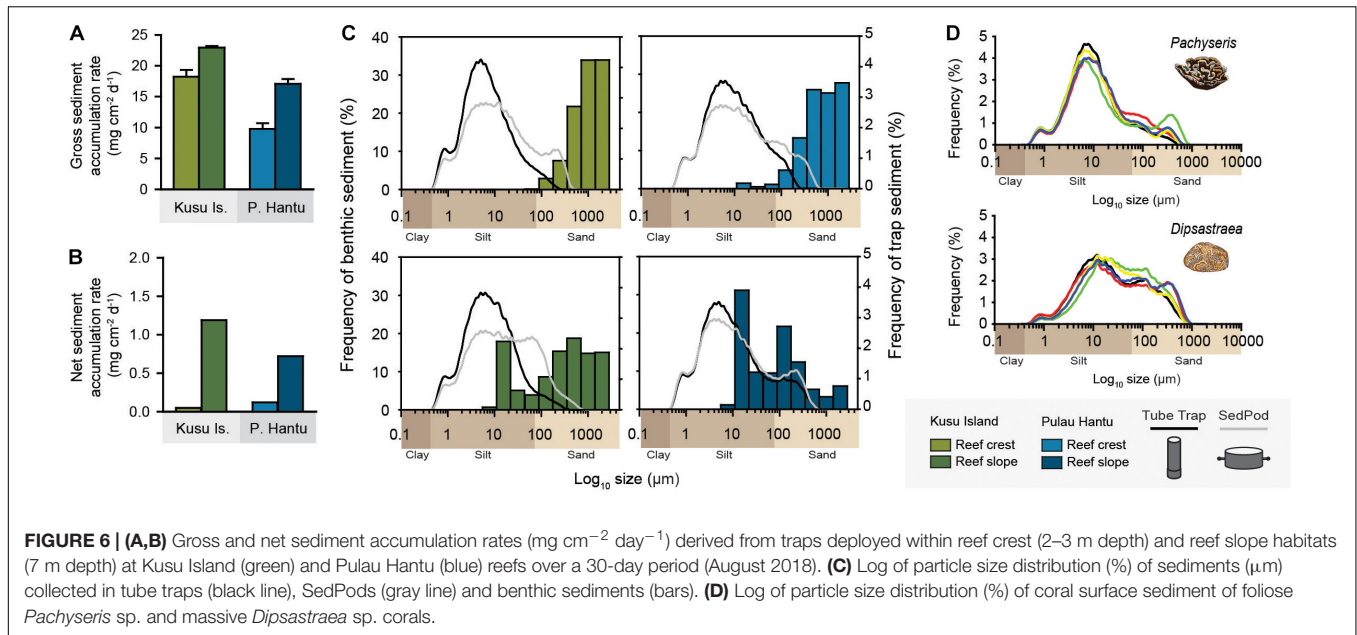
## Sediment Accumulation Rates and Grain Properties

Gross sediment accumulation rates were high at all sites ( $\geq 9.8 \text{ mg cm}^{-2} \text{ day}^{-1}$ ) and significantly greater than net sediment accumulation rates ( $p < 0.05$ ,  $t$ -test; Figures 6A,B). Highest gross sediment accumulation was recorded at Kusu. At both reefs, gross sediment accumulation was higher on the reef slope (Kusu:  $22.9 \pm 0.3 \text{ mg cm}^{-2} \text{ day}^{-1}$ ; Hantu:  $17.1 \pm 0.8 \text{ mg cm}^{-2} \text{ day}^{-1}$ ) than the reef crest (Kusu:  $18.2 \pm 4.2 \text{ mg cm}^{-2} \text{ day}^{-1}$ ; Hantu:  $9.8 \pm 0.9 \text{ mg cm}^{-2} \text{ day}^{-1}$ ). Net sediment accumulation rates showed similar spatial trends between reefs and depth zones, but were  $\sim 5\%$  of gross sediment accumulation for the same location ( $0.1$ – $1.2 \text{ mg cm}^{-2} \text{ day}^{-1}$ ; Figure 6B).

Grain size analysis showed that tube trap and SedPods sediment was dominated by silt-sized particles ( $< 63 \mu\text{m}$ ; tube traps: 86–96%; SedPods: 80–83%), with mean grain sizes of between 6.2–8.8  $\mu\text{m}$  (average:  $8.17 \pm 1.2 \mu\text{m}$ ) and 9.51–15.5  $\mu\text{m}$  (average:  $13.2 \pm 2.5 \mu\text{m}$ ), respectively (Supplementary Table 4). Grain size distributions differed between trapping methods (Figure 6C). Tube traps sediments were unimodal with a dominant peak at 7  $\mu\text{m}$  (fine silt), whereas SedPods were typically bimodal, exhibiting a lower peak at 7  $\mu\text{m}$  (fine silt) and a secondary peak at 250  $\mu\text{m}$  (fine sand). Sediments were primarily non-reef derived particles (tube traps: 80–84%; SedPods: 77–79%), with a relatively high TOC content (tube traps: 13–15%; SedPods: 13%), and a small proportion of TIC (i.e., reef-derived carbonate) (tube traps: 2–6%; SedPods: 7–9%). Coral surface sediment showed close similarities in mean grain sizes between replicate corals within the same genera (Figure 6D), but grain sizes were distinct between foliose *Pachyseris* sp. (10.78  $\mu\text{m}$ ) and massive *Dipsastraea* sp. (28.3  $\mu\text{m}$ ). Interestingly, foliose *Pachyseris* sp. had a very similar grain size distribution to tube trap sediments, which were dominated by fine silt particles, whereas massive *Dipsastraea* sp. had a coarser silt-to-sand grain size distribution that aligned closely with sediments deposited on SedPods (Figure 6).

In contrast, reef crest benthic sediments were dominated by allochthonous gravels ( $> 1000 \mu\text{m}$ ; coral, molluscan and octocoral grains) and fine-to-coarse (125–750  $\mu\text{m}$ ) sand (Figure 6C). Mean grain sizes of benthic sediment differed between reefs and depth zones (Supplementary Table 4). Benthic reef crest sediments were coarser at Kusu compared to Hantu (1093 and 524  $\mu\text{m}$ , respectively), and reef crest sediments at both reefs were coarser than those on the reef slope (314 and 183  $\mu\text{m}$ , respectively). Differences in mean grain size between depth zones were driven by the relative absence in silt particles on the reef crests, which only accounted for 1–7% of the total sediment, compared to the reef slope sediment, which comprised 29% (Kusu) and 48% (Hantu) of the total benthic sediment (Supplementary Table 4).





## Reef Sediment Dynamics

Silt particles within reef crest and reef slope benthic sediments were larger in size (medium to coarse silt) than those collected in/on traps (very fine to fine silt; **Figure 6C**). Resuspension rates were higher at the reef crest (Kusu:  $21.7 \text{ mg day}^{-1}$ ; Hantu:  $18.1 \text{ mg day}^{-1}$ ) than the reef slope (Kusu:  $16.3 \text{ mg day}^{-1}$ ; Hantu:  $9.6 \text{ mg day}^{-1}$ ), matching differences in maximum current velocities ( $CV_{max}$ ) between these sites. A wider grain size range was resuspended at reef crest sites (up to  $22.4$  and  $39.9 \mu\text{m}$  at Kusu and Hantu, respectively), whereas on the reef slope, particle size ranges were restricted to finer particles (up to  $12.6$  and  $14.2 \mu\text{m}$  at Kusu and Hantu reefs, respectively). Importantly, maximum  $CV_{max}$  was observed only 0.2–5.4% of the total time during the 30-day deployment period for both crest and slope environments (**Supplementary Table 5**).

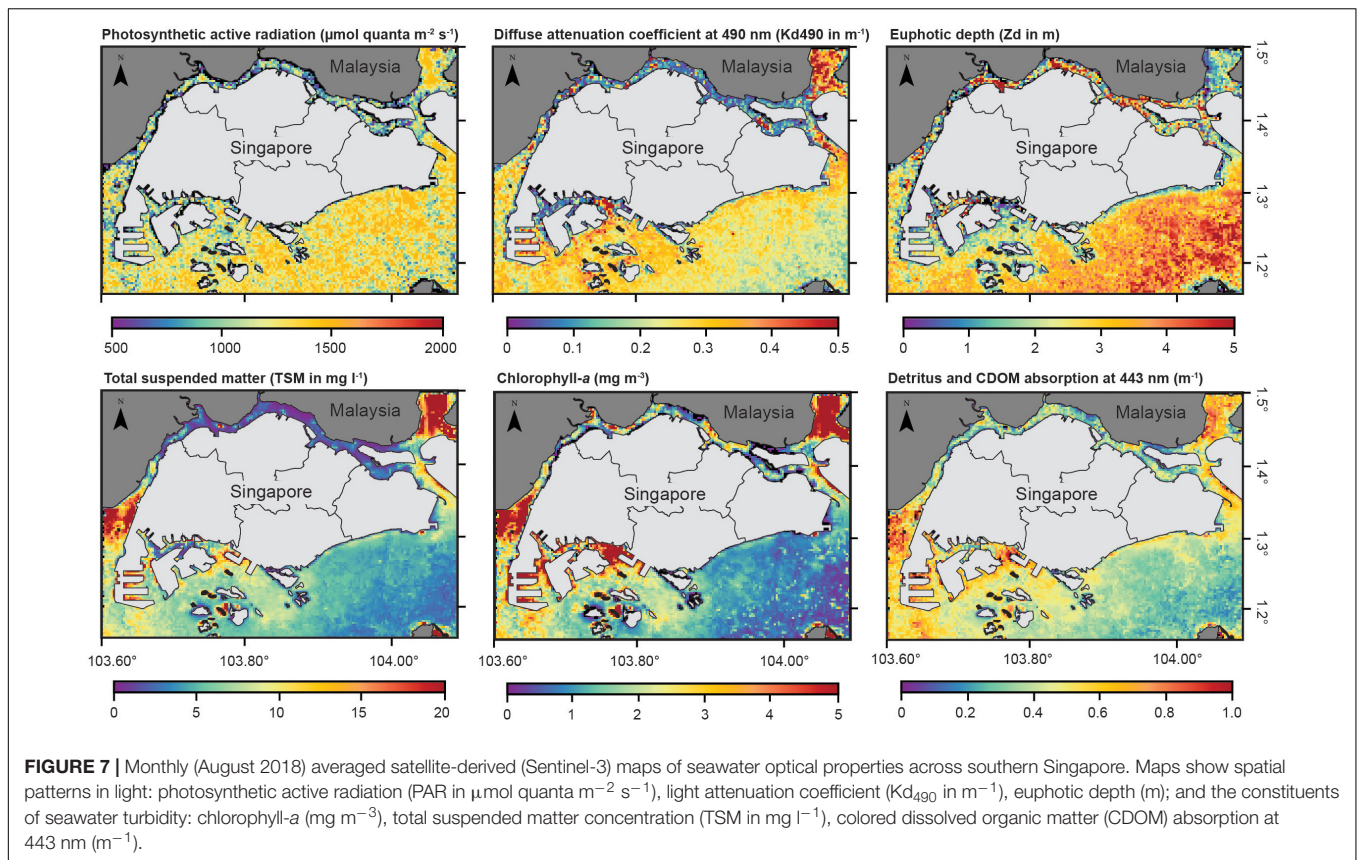
## Spatial Distribution of Light and Turbidity Across Southern Singapore

Monthly averaged (August 2018) seawater optical properties across southern Singapore are consistent with field measurements at Kusu and Hantu. Spatial maps of  $Kd_{490}$ , a proxy for turbidity, show high light attenuation ( $\sim 0.5 \text{ m}^{-1}$ ) and a shallow euphotic depth ( $Z_d$ ) of  $< 7 \text{ m}$  across southern Singapore (**Figure 7**). Spatial patterns in PAR align with  $Kd_{490}$ , as higher PAR was observed in waters surrounding Kusu ( $\sim 1500 \mu\text{mol quanta m}^{-2} \text{ s}^{-1}$ ) than Hantu ( $\sim 800 \mu\text{mol quanta m}^{-2} \text{ s}^{-1}$ ). Overall, remote sensing analysis demonstrates that Hantu received lower light intensity and had a shallower euphotic depth compared to Kusu because of the higher rate of light attenuation. Remote sensing analysis across the wider Singapore region indicated that spatial differences in  $Kd_{490}$  and PAR corresponded with higher concentrations of total suspended matter (TSM) surrounding Hantu and its nearby reefs (as evident in **Figure 7**) and that TSM declines eastward

towards Kusu. Turbidity is therefore modulated in part by chlorophyll-*a* and CDOM, which exhibit similar spatial patterns to TSM. However, chlorophyll-*a* concentrations are relatively low compared to CDOM, and thus, light attenuation is controlled by a combination of CDOM and suspended sediment, particularly at western locations during this time period.

## DISCUSSION

We provide a high-resolution times series of light and turbidity for Singapore's coral reefs, and present a process-based interpretation of the factors contributing to vertical reef compression on turbid reefs using additional physical parameters. We show that rapid light attenuation through seawater, as a function of high turbidity ( $10\text{--}50 \text{ mg l}^{-1}$ ), is a critical control restricting the maximum depth of coral growth and bioconstruction. Light conditions on Singapore's reefs were low and had high temporal variability over the 30-day deployment period in the absence of seasonality. Reductions in instantaneous PAR and DLI aligned with periods of increased turbidity (lasting 1–3 days) that reached up to  $118$  and  $230 \text{ mg l}^{-1}$  at Kusu and Hantu, respectively. Deeper reef slope sites experienced very low light or “twilight” conditions ( $\leq 0.8 \text{ DLI}$ ) (Jones et al., 2015) on 31% of days at Kusu and 91% of days at Hantu. These data highlight the marginal, and fluctuating, conditions on turbid reefs that are distinct from clear-water reefs (Burt et al., 2020), as well as the complexities of establishing relevant baseline environmental data to characterize these systems. Light levels were consistent with other turbid reef environments, where data is available (Macdonald, 2015; Morgan et al., 2017; Chow et al., 2019; Loiola et al., 2019), but we found substantial differences in irradiance levels between reefs of close proximity ( $\sim 12 \text{ km}$ ) and a similar distance offshore ( $\sim 5 \text{ km}$ ). These differences can be attributed to higher



background seawater turbidity at Hantu compared to Kusu, and to a lesser degree, may reflect differences in reef elevation. Spatial patterns in turbidity and light regimes contrast more well-established inshore-offshore water quality gradients that occur over larger spatial scales (e.g., Great Barrier Reef, Fabricius et al., 2016; Jakarta Bay, Cleary et al., 2016), and may give insight into the source of turbidity on reefs in Singapore.

Monthly-averaged remote sensing analysis supports a regional west-to-east gradient in ocean optical properties within southern Singapore (Figure 7), consistent with field measurements. Although this data provides a coarser measure of light and turbidity on reefs, it allows for interpretations to be made over greater spatial scales. Western islands that experience stronger tidal flows, caused by the funneling of water through adjacent reef structures (e.g., Pulau Hantu, Semakau and Terumbu Pempang), exhibited higher turbidity and lower light (Chen et al., 2005). In contrast, more exposed eastern reefs (e.g., Kusu, Sister's and St John's Islands) were subject to lower turbidity and higher light conditions. As different suspended particles can have varying effects on light attenuation (Storlazzi et al., 2015), and for coral health (Fabricius et al., 2003; Weber et al., 2006; Bainbridge et al., 2012; Duckworth et al., 2017), it is critical to characterize the water column components that limit light on reefs. Both optical analysis and field data showed that siliciclastic sediment particles are the main component of seawater turbidity. However, the spatial distribution of TSM also coincides with elevated concentrations of chlorophyll-*a* and CDOM, indicating that

although recent coastal development in Singapore (e.g., land reclamation, seafloor dredging) may have contributed to vertical reef compression by increasing suspended sediment (Low and Chou, 1994; Erftemeijer et al., 2012), total light attenuation on reefs is also driven by other background constituents which operate over greater spatial scales. For example, satellite remote sensing has demonstrated that high CDOM around Sumatra reaches the Malacca Straits (Siegel et al., 2018), and influences the Singapore Straits waters (Liew and Kwoh, 2003). The relatively low chlorophyll-*a* concentration around Singapore (Figure 7) confirms that light attenuation was dominated by a combination of CDOM absorption, probably from terrestrial sources, and sediment scattering that both likely vary with monsoon seasonality.

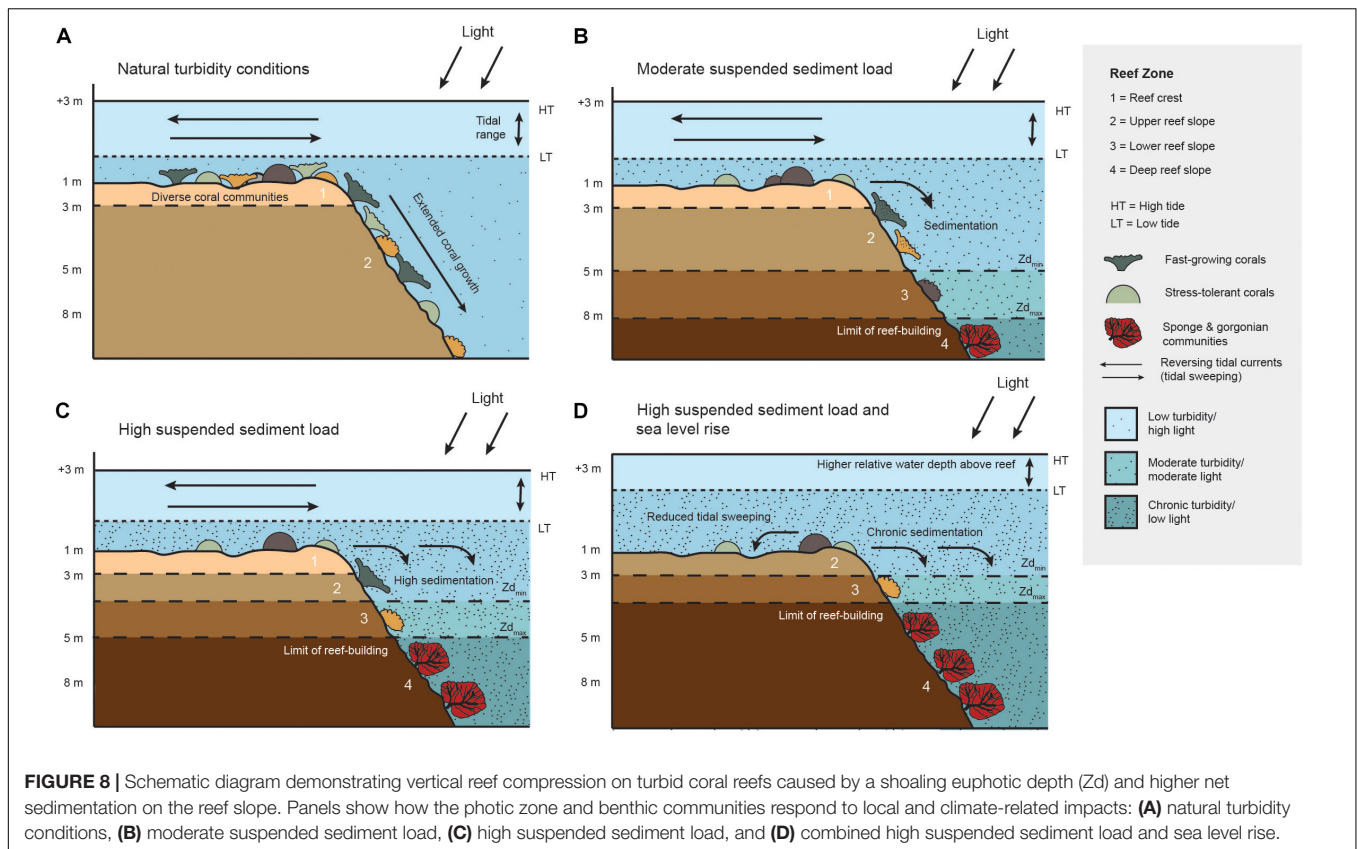
Light attenuation curves demonstrated that downwelling irradiance was rapid at both sites ( $K_{dPAR}$ :  $0.49\text{--}0.57 \text{ m}^{-1}$ ), but also highly responsive to localized conditions on reefs (Figure 4). The values of  $K_{dPAR}$  we observed on Singapore's reefs far exceeded global values from a wide geographic range of clear-water reef settings ( $0.045\text{--}0.071 \text{ m}^{-1}$ ; see Laverick et al., 2020), as well as those from other turbid reef environments ( $0.08\text{--}0.11 \text{ m}^{-1}$  at the Abrolhos complex, Brazil; Freitas et al., 2019). These values were primarily attributed to high suspended sediment in the water, which was compounded by the dominance of dark-colored siliciclastic particles that absorb light more effectively than lighter (in color) carbonate sediments (Storlazzi et al., 2015). As a result, the euphotic depth (Zd) on Singapore's

reefs is very shallow, but migrates daily as much as 3–8 m ( $\pm 11\%$  average change). The depth distribution of coral species on Singapore's reefs are well documented and show declining live coral, species richness and diversity over a short vertical range, with a maximum depth of 10 m (Chow et al., 2019). Long-term survey data also suggest low and declining coral cover at the photic floor (Guest et al., 2016). These data are consistent with our own observations of reef slope communities ( $\sim 5$  m at Hantu and  $\sim 7$  m at Kusu), which align with the minimum euphotic depth ( $Z_{d_{min}}$ ) rather than the maximum values ( $Z_{d_{max}}$ ) we recorded (Figure 4). Below  $Z_{d_{min}}$ , hard coral assemblages transition to non-phototrophic sponge and gorgonian communities with limited reef-building potential (Supplementary Figure 1). For comparison, a recent global analysis showed that transitions to mesophotic coral ecosystems typically occurred between  $36.1 \pm 5.6$  m (shallow-upper mesophotic) and  $61.9 \pm 9.6$  m (upper-lower mesophotic) (Laverick et al., 2020). Our time series of light analysis provides additional support for the classification of turbid reefs as “shallow-water mesophotic reefs” (*sensu* Morgan et al., 2016), because despite their shallow depth ( $< 10$  m) these reefs share key characteristics in both light conditions and ecological communities, where light limitation is the major driver structuring benthic assemblages.

Light effects on benthic communities are compounded by depth-related differences in sedimentation rates (Figure 6). Our combined datasets suggest vertical reef compression in turbid settings is also a consequence of sediment dynamics. High velocity tidal currents winnow fine particles from the reef crest, defined here as “tidal sweeping”, and greater silt deposition occurs on reef slopes. This process is also likely an important driver of localized turbidity at the reef-scale that often differs from off-reef conditions. Given the high background suspended sediment concentrations, tidal sweeping helps maintain the ecological stability of shallow-water corals (2–3 m) in Singapore, as strong diurnal tidal flows keep fine sediments in suspension (Maxwell, 1968; Cacciapaglia and van Woesik, 2015). Evidence of this winnowing effect on Singapore's reefs include: (1) higher measured resuspension rates and current velocities on the reef crest, (2) relatively low silt in reef crest benthic sediment ( $< 7\%$ ) and a high relative abundance of silt on the reef slope (29–48%), typical of a depositional fore-reef slope setting (e.g., Morgan and Kench, 2014), (3) a coarser silt mean grain size in benthic and SedPod sediment within the reef crest, and (4) a 20% increase in soft sediment benthic cover on reef slopes (Guest et al., 2016). We also found large differences between net and gross sedimentation rates on reefs (Figure 6), and emphasize that net sedimentation derived from SedPods (Field et al., 2013) provide a more realistic estimate of sediment deposition and retention. Here, net sedimentation values from SedPods were  $\sim 5\%$  of gross rates derived from tube traps, and deposit an additional  $4 \text{ kg m}^{-2}$  of silt-sized sediment to reef slopes annually. If gross sedimentation rates at Kusu were applied, this would equate to an overestimation of  $66 \text{ kg m}^{-2} \text{ year}^{-1}$  ( $66.4 \text{ kg m}^{-2} \text{ year}^{-1}$  versus  $0.36 \text{ kg m}^{-2} \text{ year}^{-1}$ ) on the reef crest and  $80 \text{ kg m}^{-2} \text{ year}^{-1}$  on the slope ( $83.5 \text{ kg m}^{-2} \text{ year}^{-1}$  versus  $4.38 \text{ kg m}^{-2} \text{ year}^{-1}$ ).

Our data suggests that vertical reef compression is being driven from the bottom-up, as the photic zone contracts and fine silts accumulate at depth (Figure 8), reducing both habitat availability and coral diversity (e.g., Morgan et al., 2020). Sediment deposited on reef slope corals had distinct size distributions, which replicated those exhibited by gross and net sedimentation trapping methods (Figure 6). Morphology-specific grain size ranges were likely a result of colony-level differences in water flow (Hench and Rosman, 2013; Duckworth et al., 2017), whereby foliose taxa (*Pachyseris* sp.) trap fine silt particles and massive growth forms (*Dipsastraea* sp.) trap silt and fine sand. Smothering of corals by sediment has been shown to preferentially occur on encrusting and foliose (but not branching) growth forms under periods of chronic sedimentation (Jones et al., 2020). Singapore's coral communities are dominated by encrusting, massive and foliose forms, whereas branching species (e.g., *Acropora* spp.) are largely devoid on reefs. This may make reef slope coral communities more vulnerable to sedimentation effects, as corals shift to flatter horizontal morphologies with depth to increase light capture. Although certain colony-level mechanisms (e.g., sacrificial zones, surface inclination) can help mitigate the effects of sediment smothering on corals (Jones et al., 2019), field observations indicate sediment loading occurs on reef slope colonies. Therefore, the ability of reef currents to sort sediment particles deposited on coral surfaces has important implications, because sediment impacts are strongly influenced by sediment type (Te, 1992; Duckworth et al., 2017). While the physical properties of the suspended sediment in Singapore may pose a greater threat to complex coral morphologies, the ultimate influence of coral-sediment interactions depends on the total magnitude of reef sedimentation.

Our process-based assessment of vertical reef compression on turbid coral reefs is critical for understanding the response of benthic communities to future local and global environmental change (Figure 8). Under naturally turbid conditions, light propagates deeper to extend the depth range of coral growth, with diverse benthic communities and complex reef framework on the slope (Figure 8A). Localized increases in suspended particles reduce light penetration to shoal the euphotic zone, and coral communities transition to stress-tolerant and low-profile taxa (Morgan et al., 2016; Perry and Alvarez-Filip, 2018). Tidal sweeping can maintain reef crest communities by limiting sedimentation, but high sedimentation on reef slopes reduces available coral habitat (Figure 8B). Further declines in water quality can dramatically compress the zone of active reef growth (Figure 8C), as suspended particles adsorb light and greater sediment accumulation on reef slopes convert more benthic surfaces to soft-sediment. Under higher future sea levels associated with global climate change (Figure 8D), estimated deficits between vertical reef accretion by living coral communities ( $1.29 \pm 0.20 \text{ mm year}^{-1}$ ) and projected sea level rise ( $3.0 \pm 1.3 \text{ mm year}^{-1}$ ) in Singapore suggest water depths could increase by 20–60 cm in the next 80 years (Tkalic et al., 2013; Januchowski-Hartley et al., 2020). Raising of the euphotic depth by this amount will compress available reef habitat by 8–12% assuming no additional declines in water quality. A higher sea level may also affect reef crest sediment dynamics, including



tidal sweeping, to further elevate turbidity. For example, an observation-based study predicted a doubling in the average daily maximum suspended sediment concentration ( $11\text{--}20\text{ mg l}^{-1}$ ) with a 20 cm sea level rise (Ogston and Field, 2010). If projected relative water level changes occur in synergy with intensified local stressors, reef communities may become highly fragmented and ecologically redundant due to an increasing lack of light and a greater abundance of soft-sediment benthic cover.

## CONCLUSION

Current understanding of vertical reef compression on turbid reefs remains largely speculative, or overly simplified, because of insufficient field data. Here, we find that on turbid coral reefs in Singapore, the depth range available for coral growth is shallow ( $<11\text{ m}$ ) and determined by: (1) rapid attenuation of PAR over short depth ranges and (2) depth-related differences in reef hydrodynamics and sedimentation. Light attenuation is driven by suspended particulate matter in the water column, comprised of sediment, chlorophyll-*a* and CDOM, which dramatically shoals the euphotic depth. Reef slopes experience high net sedimentation of siliciclastic silt particles, which smother consolidated substrates and reduce available coral habitat. Critically, coral morphology influences the type and particle size of sediment deposited on coral surfaces. Our findings support reported ecological patterns for Singapore's reefs over the past 27 years, where reef crest corals have retained relative ecological

stability as tidal sweeping removes excess silt particles, and slope communities have converted to soft-sediment benthic cover. This suggests that turbid coral communities, in particular deeper corals at the photic floor, are highly vulnerable to the synergistic effects of local anthropogenic stressors and future sea level rise.

## DATA AVAILABILITY STATEMENT

The raw data supporting the conclusions of this article will be made available by the authors, without undue reservation.

## AUTHOR CONTRIBUTIONS

KM conceived and designed the project and conducted the sediment analysis. KM and MM carried out the fieldwork. KM and NS undertook the data analysis. NS performed the remote sensing. KM prepared the manuscript, with contributions by MM, NS, and AS. All authors gave their final approval for publication.

## FUNDING

This research was supported by Singapore's National Research Foundation (NRF) under the Marine Science Research and Development Programme (MSRDP-P11). KM is a beneficiary

of an AXA Research Fund Postdoctoral Grant and a Nanyang Presidential Postdoctoral Research Fellowship.

## ACKNOWLEDGMENTS

We would like to acknowledge the crew of Dolphin Explorer for their assistance during fieldwork. Research was carried out under Singapore National Park Board permit (NP/RP17-044a).

## REFERENCES

- Anthony, K. R., Hoogenboom, M. O., and Connolly, S. R. (2005). Adaptive Variation in Coral geometry and the optimization of internal colony light climates. *Funct. Ecol.* 19, 17–26. doi: 10.1111/j.0269-8463.2005.00925.x
- Bainbridge, Z. T., Wolanski, E., Álvarez-Romero, J. G., Lewis, S. E., and Brodie, J. E. (2012). Fine sediment and nutrient dynamics related to particle size and floc formation in a Burdekin River flood plume. *Austr. Mar. Pollut. Bull.* 65, 236–248. doi: 10.1016/j.marpolbul.2012.01.043
- Bainbridge, Z., Lewis, S., Bartley, R., Fabricius, K., Collier, C., Waterhouse, J., et al. (2018). Fine sediment and particulate organic matter: A review and case study on ridge-to-reef transport, transformations, fates, and impacts on marine ecosystems. *Mar. Pollut. Bull.* 135, 1205–1220. doi: 10.1016/j.marpolbul.2018.08.002
- Baum, G., Januar, H. I., Ferse, S. C. A., and Kunzmann, A. (2015). Local and regional impacts of pollution on coral reefs along the thousand islands north of the megacity Jakarta. *Indonesia. PLoS One* 10:e0138271. doi: 10.1371/journal.pone.0138271
- Bellwood, D. R., and Hughes, T. P. (2001). Regional-scale assembly rules and biodiversity of coral reefs. *Science* 292, 1532–1534. doi: 10.1126/science.1058635
- Blott, S., and Pye, K. (2001). GRADISTAT: a grain size distribution and statistics package for the analysis of unconsolidated sediments. *Earth Surf. Process. Landforms*. 26, 1237–1248.
- Brockmann, C., Doerffer, R., Peters, M., Stelzer, K., Embacher, S., and Ruescas, A. (2016). Evolution of the C2RCC neural network for Sentinel 2 and 3 for the retrieval of ocean colour products in normal and extreme optically complex waters. *Eur. Space Agency*. 740:54.
- Browne, N. K., Tay, J. K. L., Low, J., Larson, O., and Todd, P. A. (2015). Fluctuations in coral health of four common inshore reef corals in response to seasonal and anthropogenic changes in water quality. *Mar. Environ. Res.* 105, 39–52. doi: 10.1016/j.marenvres.2015.02.002
- Burke, L., Reyter, K., Spalding, M., and Perry, A. (2011). *Reefs at Risk Revisited*. Washington, D C: World Resources Institute.
- Burt, J. A., Camp, E. F., Enochs, I. C., Johansen, J. L., Morgan, K. M., Riegl, B., et al. (2020). Insights from extreme coral reefs in a changing world. *Coral Reefs*. 39, 495–507. doi: 10.1007/s00338-020-01966-y
- Cacciapaglia, C., and van Woesik, R. (2015). Reef-coral refugia in a rapidly changing ocean. *Glob. Chang. Biol.* 21, 2272–2282. doi: 10.1111/gcb.12851
- Chen, M., Murali, K., Khoo, B.-C., Lou, J., and Kumar, K. (2005). Circulation Modelling in the Strait of Singapore. *J. Coast. Res.* 215, 960–972. doi: 10.2112/04-0412.1
- Cheng, N.-S. S., and Chiew, Y.-M. M. (1999). Analysis of initiation of sediment suspension from bed load. *J. Hydraul. Eng.* 125, 855–861. doi: 10.1061/(ASCE)0733-94291999125:8(855)
- Chow, G. S. E., Chan, Y. K. S., Jain, S. S., and Huang, D. (2019). Light limitation selects for depth generalists in urbanised reef coral communities. *Mar. Environ. Res.* 147, 101–112. doi: 10.1016/j.marenvres.2019.04.010
- Cleary, D. F. R., Polónia, A. R. M., Renema, W., Hoeksema, B. W., Racheo-Dolmen, P. G., Moolenbeek, R. G., et al. (2016). Variation in the composition of corals, fishes, sponges, echinoderms, ascidians, molluscs, foraminifera and macroalgae across a pronounced in-to-offshore environmental gradient in the Jakarta Bay–Thousand Islands coral reef complex. *Mar. Pollut. Bull.* 110, 701–717. doi: 10.1016/j.marpolbul.2016.04.042

We would like to thank the reviewers for their thoughtful and constructive comments.

## SUPPLEMENTARY MATERIAL

The Supplementary Material for this article can be found online at: <https://www.frontiersin.org/articles/10.3389/fmars.2020.571256/full#supplementary-material>

- de Soares, M. O. (2020). Marginal reef paradox: A possible refuge from environmental changes? *Ocean Coast. Manag.* 185:105063. doi: 10.1016/j.ocecoaman.2019.105063
- Doerffer, R., and Schiller, H. (2007). The MERIS case 2 water algorithm. *Int. J. Remote Sens.* 28, 517–535. doi: 10.1080/01431160600821127
- Duckworth, A., Giofre, N., and Jones, R. (2017). Coral morphology and sedimentation. *Mar. Pollut. Bull.* 125, 289–300. doi: 10.1016/j.marpolbul.2017.08.036
- Duprey, N. N., Wang, T. X., Kim, T., Cybulski, J. D., Vonhof, H. B., Crutzen, P. J., et al. (2020). Megacity development and the demise of coastal coral communities: Evidence from coral skeleton  $\delta^{15}\text{N}$  records in the Pearl River estuary. *Glob. Chang. Biol.* 26, 1338–1353. doi: 10.1111/gcb.14923
- Erfteimeijer, P. L. A., Riegl, B., Hoeksema, B. W., and Todd, P. A. (2012). Environmental impacts of dredging and other sediment disturbances on corals: A review. *Mar. Pollut. Bull.* 64, 1737–1765. doi: 10.1016/j.marpolbul.2012.05.008
- Fabricius, K. E. (2005). Effects of terrestrial runoff on the ecology of corals and coral reefs: review and synthesis. *Mar. Pollut. Bull.* 50, 125–146. doi: 10.1016/j.marpolbul.2004.11.028
- Fabricius, K. E., Logan, M., Weeks, S. J., Lewis, S. E., and Brodie, J. (2016). Changes in water clarity in response to river discharges on the Great Barrier Reef continental shelf: 2002–2013. *Estuar. Coast. Shelf Sci.* 173, A1–A15. doi: 10.1016/j.ecss.2016.03.001
- Fabricius, K. E., Wild, C., Wolanski, E., and Abele, D. (2003). Effects of transparent exopolymer particles and muddy terrigenous sediments on the survival of hard coral recruits. *Estuar. Coast. Shelf Sci.* 57, 613–621. doi: 10.1016/S0272-7714(02)00400-6
- Field, M. E., Chezar, H., and Storlazzi, C. D. (2013). SedPods: A low-cost coral proxy for measuring net sedimentation. *Coral Reefs* 32, 155–159. doi: 10.1007/s00338-012-0953-5
- Freitas, L. M., Oliveira, M., de, D. M., Leão, Z. M. A. N., and Kikuchi, R. K. P. (2019). Effects of turbidity and depth on the bioconstruction of the Abrolhos reefs. *Coral Reefs* 38, 241–253. doi: 10.1007/s00338-019-01770-3
- Gibbs, R. J., Matthews, M. D., and Link, D. A. (1971). The Relationship Between Sphere Size And Settling Velocity. *SEPM J. Sediment. Res.* 41, 7–18. doi: 10.1306/74D721D0-2B21-11D7-8648000102C1865D
- Goodkin, N. F., Switzer, A. D., McCorry, D., DeVantier, L., True, J. D., Hughen, K. A., et al. (2011). Coral communities of Hong Kong: Long-lived corals in a marginal reef environment. *Mar. Ecol. Prog. Ser.* 426, 185–196. doi: 10.3354/meps09019
- Guest, J. R., Baird, A. H., Maynard, J. A., Muttaqin, E., Edwards, A. J., Campbell, S. J., et al. (2012). Contrasting patterns of coral bleaching susceptibility in 2010 suggest an adaptive response to thermal stress. *PLoS One* 7:e33353. doi: 10.1371/journal.pone.0033353
- Guest, J. R., Tun, K., Low, J., Vergés, A., Marzinelli, E. M., Campbell, A. H., et al. (2016). 27 years of benthic and coral community dynamics on turbid, highly urbanised reefs off Singapore. *Sci. Rep.* 6:36260. doi: 10.1038/srep36260
- Heery, E. C., Hoeksema, B. W., Browne, N. K., Reimer, J. D., Ang, P. O., Huang, D., et al. (2018). Urban coral reefs: Degradation and resilience of hard coral assemblages in coastal cities of East and Southeast Asia. *Mar. Pollut. Bull.* 135, 654–681. doi: 10.1016/j.marpolbul.2018.07.041
- Heiri, O., Lotter, A. F., and Lemcke, G. (2001). Loss on ignition as a method for estimating organic and carbonate content in sediments: Reproducibility

- and comparability of results. *J. Paleolimnol.* 25, 101–110. doi: 10.1023/A:1008119611481
- Hench, J. L., and Rosman, J. H. (2013). Observations of spatial flow patterns at the coral colony scale on a shallow reef flat. *J. Geophys. Res. Ocean.* 118, 1142–1156. doi: 10.1002/jgrc.20105
- Hilton, M. J., and Ming, C. L. (1999). Sediment facies of a low-energy, meso-tidal, fringing reef. *Singap. J. Trop. Geogr.* 20, 111–130. doi: 10.1111/1467-9493.00049
- Hinrichsen, D. (2016). *Our common seas: Coasts in crisis*. London: Routledge.
- Hughes, T. P., Anderson, K. D., Connolly, S. R., Heron, S. F., Kerry, J. T., Lough, J. M., et al. (2018). Spatial and temporal patterns of mass bleaching of corals in the Anthropocene. *Science* 359, 80–83. doi: 10.1126/science.aan8048
- Januchowski-Hartley, F. A., Bauman, A. G., Morgan, K. M., Seah, J. C. L., Huang, D., and Todd, P. A. (2020). Accreting coral reefs in a highly urbanized environment. *Coral Reefs* 39, 717–731. doi: 10.1007/s00338-020-01953-3
- Jones, R., Bessell-Browne, P., Fisher, R., Klonowski, W., and Slivkoff, M. (2016). Assessing the impacts of sediments from dredging on corals. *Mar. Pollut. Bull.* 102, 9–29. doi: 10.1016/j.marpollbul.2015.10.049
- Jones, R., Fisher, R., and Bessell-Browne, P. (2019). Sediment deposition and coral smothering. *PLoS One* 14, 1–24. doi: 10.1371/journal.pone.0216248
- Jones, R., Fisher, R., Stark, C., and Ridd, P. (2015). Temporal patterns in seawater quality from dredging in tropical environments. *PLoS One* 10, 1–25. doi: 10.1371/journal.pone.0137112
- Jones, R., Giofre, N., Luter, H. M., Neoh, T. L., Fisher, R., and Duckworth, A. (2020). Responses of corals to chronic turbidity. *Sci. Rep.* 10, 1–13. doi: 10.1038/s41598-020-61712-w
- Kamp-Nielsen, L., Vermaat, J. E., Wesseling, I., Borum, J., and Geertz-Hansen, O. (2002). Sediment properties along gradients of siltation in south-east Asia. *Estuar. Coast. Shelf Sci.* 54, 127–137. doi: 10.1006/ecss.2001.0822
- Lai, S., Loke, L. H. L., Hilton, M. J., Bouma, T. J., and Todd, P. A. (2015). The effects of urbanisation on coastal habitats and the potential for ecological engineering: A Singapore case study. *Ocean Coast. Manag.* 103, 78–85. doi: 10.1016/j.ocecoaman.2014.11.006
- Laverick, J. H., Tamir, R., Eyal, G., and Loya, Y. (2020). A generalized light-driven model of community transitions along coral reef depth gradients. *Glob. Ecol. Biogeogr.* 29, 1554–1564. doi: 10.1111/geb.13140
- Liew, S. C., and Kwoh, L. K. (2003). *Mapping Optical Parameters of Coastal Sea Waters using the Hyperion Imaging Spectrometer: Intercomparison with MODIS Ocean Color Products*. New Jersey, NJ: IEEE.
- Loiola, M., Cruz, I. C. S., Lisboa, D. S., Mariano-Neto, E., Leão, Z. M. A. N., Oliveira, M. D. M., et al. (2019). Structure of marginal coral reef assemblages under different turbidity regime. *Mar. Environ. Res.* 147, 138–148. doi: 10.1016/j.marenvres.2019.03.013
- Low, J. K. Y., and Chou, L. M. (1994). “Sedimentation rates in Singapore waters,” in *Proceedings, Third ASEAN-Australia Symposium on Living Coastal Resources*. (Bangkok: Chulalongkorn University), 697–701.
- Macdonald, R. K. (2015). *Turbidity and light attenuation in coastal waters of the Great Barrier Reef*. Thesis, Mackay: James Cook University, 232.
- Maxwell, W. (1968). *Atlas of the Great Barrier Reef*. Available online at: <http://agris.fao.org/agris-search/search.do?recordID=XF2017003063> (accessed June 7, 2020).
- Morgan, K. M. M., and Kench, P. S. S. (2014). A detrital sediment budget of a Maldivian reef platform. *Geomorphology* 222, 122–131. doi: 10.1016/j.geomorph.2014.02.013
- Morgan, K. M., and Kench, P. S. (2016). Reef to island sediment connections on a Maldivian carbonate platform: using benthic ecology and biosedimentary depositional facies to examine island-building potential. *Earth Surf. Process. Landform.* 41, 1815–1825. doi: 10.1002/esp.3946
- Morgan, K. M., Perry, C. T., Arthur, R., Williams, H. T. P., and Smithers, S. G. (2020). Projections of coral cover and habitat change on turbid reefs under future sea-level rise. *Proc. Biol. Sci.* 287:20200541. doi: 10.1098/rspb.2020.0541
- Morgan, K. M., Perry, C. T., Johnson, J. A., and Smithers, S. G. (2017). Nearshore Turbid-Zone Corals Exhibit High Bleaching Tolerance on the Great Barrier Reef Following the 2016 Ocean Warming Event. *Front. Mar. Sci.* 4:224. doi: 10.3389/fmars.2017.00224
- Morgan, K. M., Perry, C. T., Smithers, S. G., Johnson, J. A., and Daniell, J. J. (2016). Evidence of extensive reef development and high coral cover in nearshore environments: implications for understanding coral adaptation in turbid settings. *Sci. Rep.* 6:29616. doi: 10.1038/srep29616
- Ogston, A. S., and Field, M. E. (2010). Predictions of Turbidity Due to Enhanced Sediment Resuspension Resulting from Sea-Level Rise on a Fringing Coral Reef: Evidence from Molokai. *Hawaii. J. Coast. Res.* 26, 1027–1037. doi: 10.2112/jcoastres-d-09-00064.1
- Perry, C. T., and Alvarez-Filip, L. (2018). Changing geo-ecological functions of coral reefs in the Anthropocene. *Funct. Ecol.* 33, 976–988. doi: 10.1111/1365-2435.13247
- Perry, C. T., and Morgan, K. M. (2017). Bleaching drives collapse in reef carbonate budgets and reef growth potential on southern Maldives reefs. *Sci. Rep.* 7, 1–9. doi: 10.1038/srep40581
- Risk, M. J. (2014). Assessing the effects of sediments and nutrients on coral reefs. *Curr. Opin. Environ. Sustain.* 7, 108–117. doi: 10.1016/j.cosust.2014.01.003
- Saulquin, B., Hamdi, A., Gohin, F., Populus, J., Mangin, A., and D’Andon, O. F. (2013). Estimation of the diffuse attenuation coefficient KdPAR using MERIS and application to seabed habitat mapping. *Remote Sens. Environ.* 128, 224–233. doi: 10.1016/j.rse.2012.10.002
- Shaffer, J. M., and Beaulieu, J. J. (2012). Calibration of the Odyssey™ Photosynthetic Irradiance Recorder™ for absolute irradiance measures. *J. Freshw. Ecol.* 27, 599–605. doi: 10.1080/02705060.2012.711259
- Siegel, H., Gerth, M., Stottmeister, I., Baum, A., and Samiaji, J. (2018). “Remote sensing of coastal discharge of SE Sumatra (Indonesia),” in *Remote Sensing of the Asian Seas*, eds V. Barale and M. Gade (Berlin: Springer), 359–379.
- Storlazzi, C. D., Norris, B. K., and Rosenberger, K. J. (2015). The influence of grain size, grain color, and suspended-sediment concentration on light attenuation: Why fine-grained terrestrial sediment is bad for coral reef ecosystems. *Coral Reefs* 34, 967–975. doi: 10.1007/s00338-015-1268-0
- Syvitski, J. P. M., Vo, C. J., Kettner, A. J., and Green, P. (2005). Impact of humans on the flux of terrestrial sediment to the global coastal ocean. *Science* 308, 376–380.
- Te, F. T. (1992). Response to higher sediment loads by *Pocillopora damicornis* planulae. *Coral Reefs* 11, 131–134. doi: 10.1007/BF00255466
- Tkalich, P., Vethamony, P., Luu, Q. H., and Babu, M. T. (2013). Sea level trend and variability in the Singapore Strait. *Ocean Sci.* 9, 293–300. doi: 10.5194/os-9-293-2013
- Weber, M., Lott, C., and Fabricius, K. E. (2006). Sedimentation stress in a scleractinian coral exposed to terrestrial and marine sediments with contrasting physical, organic and geochemical properties. *J. Exp. Mar. Biol. Ecol.* 336, 18–32. doi: 10.1016/j.jembe.2006.04.007

**Conflict of Interest:** The authors declare that the research was conducted in the absence of any commercial or financial relationships that could be construed as a potential conflict of interest.

Copyright © 2020 Morgan, Moynihan, Sanwlan and Switzer. This is an open-access article distributed under the terms of the Creative Commons Attribution License (CC BY). The use, distribution or reproduction in other forums is permitted, provided the original author(s) and the copyright owner(s) are credited and that the original publication in this journal is cited, in accordance with accepted academic practice. No use, distribution or reproduction is permitted which does not comply with these terms.